

Optical Spectra of Candidate Southern Hemisphere International Celestial Reference Frame (ICRF) radio sources

O. Titov

Geoscience Australia, PO Box 378, Canberra, ACT 2601, Australia

oleg.titov@ga.gov.au

D. L. Jauncey

CSIRO Astronomy and Space Science, ATNF & Mount Stromlo Observatory, Cotter Road,
Weston, ACT 2611, Australia

H. M. Johnston and R. W. Hunstead

Sydney Institute for Astronomy, School of Physics, University of Sydney, NSW 2006,
Australia

and

L. Christensen

Technische Universität Munich, Excellence Cluster Universe, Boltzmannstr. 2, D-85748
Garching

Received _____; accepted _____

ABSTRACT

We present the results of spectroscopic observations of the optical counterparts of 47 southern radio sources from the candidate International Celestial Reference Catalogue (ICRC), as part of a Very Long Baseline Interferometry (VLBI) program to strengthen the celestial reference frame, especially in the south. The observations were made with the 3.58-meter European Southern Observatory New Technology Telescope (NTT). We obtained redshifts for 30 quasars and one radio galaxy, with a further 7 objects being probable BL Lac objects with featureless spectra. Of the remainder, four were clear misidentifications with Galactic stars and five had low signal-to-noise spectra and could not be classified. These results add significantly to the existing data needed to refine the distribution of source proper motions over the celestial sphere.

Subject headings: radio continuum: general — galaxies: redshifts — quasars: emission lines — reference systems

1. Introduction

We are investigating the intrinsic properties and distribution of the ultra-compact, flat-spectrum radio sources that make up the International Very Long Baseline Interferometry (VLBI) Service (IVS) Reference Catalogue. Astrometric VLBI measures precise group delays, difference in arrival times of the radio waves at widely separated radio telescopes, and thus produces accurate radio positions typically with milliarcsecond precision. The first systematic astrometric VLBI program was started in 1979 and, since 2000, IVS has organised a comprehensive international program of precision position measurements of about one thousand sources (Schlüter & Behrend 2007).

About 50 radio telescopes have participated in observations over the 30-year IVS history. Conventional reductions of high-precision multi-frequency VLBI data are made in the reference system with its origin at the barycentre of the Solar system (McCarthy & Petit 2004). This barycentric reference system was adopted by the International Astronomical Union (IAU) as the International Celestial Reference System (ICRS). By definition, the axes of the ICRS are fixed by the positions of selected extragalactic radio sources, and the reference frame representing the system should show no global rotation with respect to these sources. VLBI presently represents the most precise, practical and reliable method to realise such a catalogue.

From 1998 through 2009 the initial International Celestial Reference Frame (ICRF1) was based on a catalogue of 608 radio VLBI source positions. Of those, 212 were so-called “defining” sources that were used to establish the orientation of the ICRS axes (Ma et al. 1998). In 2009 the second realization of the ICRF (ICRF2) was put forward. ICRF2 contains 295 “defining” sources of which only 97 were “defining” in the ICRF1. The claimed formal position error of the best observed radio sources in the ICRF2 is 6–7 μas , but a more realistic “inflated” error is reported as 41 μas (Fey et al. 2009).

A separate program is underway to link the optical and radio reference frames, and one of the important tasks here is to make reliable optical identifications whenever an optical counterpart can be found. However, along the Galactic plane the high dust absorption and the high density of Galactic stars can make identification impossible. Spectroscopic observations may be able to confirm an identification but more often the field will be obscured.

The total number of radio sources included in the IVS astrometric program exceeds 4,000, though only $\sim 1,000$ sources are observed on a regular basis. The database of the radio source physical characteristics (Titov & Malkin 2009) comprises 4261 objects (by August, 2010), mostly quasars, but there is a serious deficit in the southern hemisphere of candidate sources for which VLBI observations have been made. There is also a significant lack of optical identifications for the existing candidate radio sources. By July 2010, of the 2211 ICRF2 sources with measured redshifts, only 781 are in the southern hemisphere and only 129 have declinations south of -40° . Lack of redshifts in the south can cause difficulties in the analysis of apparent proper motions of the reference radio sources (Titov & Malkin 2009).

Our spectroscopic program therefore focuses on spectroscopic observations of the IVS radio sources with optical counterparts, especially those in the south, as well as those with a long observational history. In this paper we present spectra of 44 extragalactic objects observed at the European Southern Observatory’s (ESO) 3.58-meter New Technology Telescope (NTT). We describe the data reduction and analysis procedures in Section 2 and report our results in Section 3. Throughout the paper we adopt the source names used by the IVS community; these are similar—and, in many cases, identical—to the original PKS B1950 convention.

2. Observations

The observations were carried out in 2010 August at the NTT (Visitor Mode run 085A-0588 (A)) using the ESO Faint Object Spectrograph and Camera (EFOSC) system with grism #13 covering the wavelength range 3685–9315 Å. The seeing was typically 0.8–1.5 arcseconds but occasionally as high as 4 arcseconds. The measured spectral resolution was 21 Å FWHM. After setting up on each target we observed for an initial 15 minutes, followed by an additional 15 minutes if no obvious emission line was seen on the first exposure; individual spectra were later combined. Wavelength calibration was performed using the spectrum of a He/Ne/Ar comparison lamp, resulting in typical fit errors of 0.5 Å (rms).

Data reduction was performed with the IRAF software suite using standard procedures for spectral analysis. We removed the bias and pixel-to-pixel gain variations from each frame and then removed cosmic rays using the IRAF task SZAP. The separate exposures were then combined and a single spectrum extracted. We calibrated the resulting one-dimensional spectrum in wavelength, and flux-calibrated each spectrum by comparing with the spectrum of a spectrophotometric standard taken with the same instrumental setup. Because the observing conditions were not photometric, the flux calibration should be taken as approximate.

3. Results

The outcomes from the spectroscopic observations of 47 targets were as follows (Table 1).

- Emission-line redshifts: 31

- Probable BL Lac objects: 8
- Galactic stars: 3
- Spectra with S/N too low to classify: 5

Spectra for 44 of the targets are presented in Fig. 1, and emission-line data for the 31 objects for which redshifts have been determined are given in Table 2. The radio positions were taken from the ICRF2 catalogue (Fey et al. 2009).

Seven objects—IVS B0122–260, B1443–162, B1533–316, B1633–810, B2012–017, B2053–323 and B2254–204— were found to have featureless spectra and hence are identified as probable BL Lac objects.

Four objects that were found close to the radio position were identified as stars. Two of these, IVS B1748–253 and IVS B1822–173, are within 3° of the Galactic plane, are in dense star fields and exhibit extinction in V of at least 5 magnitudes, so it remains unlikely that their actual optical counterparts will be detectable. Radio-optical position differences for all four objects are given in Table 2, and the identification is rejected on positional grounds in each case. More detailed discussion of two special cases, IVS B1923+210 and IVS B2300–307, is given in subsections 3.2 and 3.3 respectively.

Finally, there were five targets with low signal/noise spectra that could not be classified—IVS B0107–610, B1452–168, B1647–296, B1936–623 and B2059–786—due either to their faintness or poor observing conditions. The field of IVS B1647–296, at $\ell = 352^\circ.5$, $b = 9^\circ.35$, is too crowded to be confident that the object observed was the correct identification and that the spectrum was not contaminated by light from a neighbouring star.

3.1. Notes on individual sources

- IVS B0002–170 – reported as a quasar with redshift $z = 0.77539$ (Q=3) in the 6dF survey (Jones et al. 2009); our redshift of $z = 0.7804 \pm 0.0013$ is based on a much higher signal-to-noise spectrum.
- IVS B0008–300 – strong absorption feature blueward of the Ly- α emission line.
- IVS B0028–396 – only two lines were identified in a noisy spectrum but the redshift is secure.
- IVS B0055–059 – reported as a quasar with redshift $z = 1.23998$ (Q=2) in the 6dF survey (Jones et al. 2009); our redshift of $z = 1.2456 \pm 0.0008$ is more reliable because of the higher signal-to-noise spectrum.
- IVS B1707–038 – previously known as a BL Lac object (Halpern et al. 2003), but weak emission lines were clearly detected in our spectrum at $z = 1.9231$.
- IVS B1505–304 – the highest redshift object, $z = 3.40$, in this sample; strong absorption shortward of Ly- α , with Lyman limit absorption at or close to the emission redshift.
- IVS B2135–184 – original galaxy identification by Gearhart et al. (1972)
- IVS B2318–087 – Faint object, but clear emission lines of Ly- α and C IV give us confidence that our redshift of $z = 3.1639$ is correct.
- IVS B2344–514 – ICRF2 defining source. The redshift $z = 2.67$ cited by Fey et al. (2009) is not correct, possibly due to the misidentification of C IV with Ly- α

3.2. IVS B1923+210

The optical counterpart (see Fig 2, object 3) was previously observed at the Russian 6-meter telescope (Maslennikov et al. 2010), and no emission lines were found. For the current campaign we observed all three optical objects located close to the ICRF2 position at 19h 25m 59.605s +21° 06′ 26.16″ (J2000). The spectra of objects 1 and 2 both show the Ca II triplet at rest, which confirms them as stars. Object 3, which has $R \sim 20$ and is coincident with the radio position, shows no stellar absorption features although the S/N is poor. There are also no obvious emission lines. The combination of a radio-optical coincidence and featureless spectrum is sufficient to suggest this as a probable BL Lac object.

3.3. IVS B2300–307

The object closest to the Tidbinbilla interferometer position was reported as a star of magnitude 16 by Jauncey et al. (1982) despite close positional agreement. Later radio observations confirmed it as a strong source ~ 0.5 Jy with a flat spectrum (Wright et al. 1991; Quiniento & Cersosimo 1993; Reynolds et al. 1994). A VLBI image at 8.4 GHz published by Ojha et al. (2005) reveals the classical double structure of an extragalactic radio source, with components separated by $r = 3.3$ mas in positional angle 124° . Optical observations reveal a single object (Fig 3) with a stellar absorption spectrum characteristic of a G star. This star is offset by 3.7 arcseconds from the ICRF2 radio position. The VLBI radio structure of IVS B2300–307 (Ojha et al. 2005), its low radio proper motion, $15 \mu\text{as/yr}$ (Reynolds et al. 1994, IVS data from 2002), and its high brightness temperature, 10^{11}K (Preston et al. 1985) all strongly support its extragalactic nature. Therefore we conclude that the field of IVS B2300–307 is obscured by the foreground star. Since there is no sign of an extra image at the precise ICRF2 position, marked with a cross in Fig. 3, we estimate

that the optical counterpart probably has $B \geq 21$.

4. Comparison of radio and optical positions

Correct identification of extragalactic radio sources can be also verified by comparison of their optical and radio coordinates. In our case we compared radio coordinates from ICRF2 and optical coordinates from the SuperCOSMOS survey (Hambly et al. 2001). Of the 31 extragalactic sources, positions for only 25 could be accurately determined; the remainder were excluded, either because the images were too faint to be measured reliably by SuperCOSMOS, or were blended because of low Galactic latitude. Two low-redshift objects (IVS B2135–184 and B2211–388) were excluded because their images were clearly non-stellar. We found the mean difference between the radio and optical position to be $0''.064 \pm 0''.021$ with $1\text{-}\sigma$ rms of $0''.103$ in right ascension and $0''.023 \pm 0''.031$ with $1\text{-}\sigma$ rms of $0''.155$ in declination. The scatter in both coordinates is small and supports the claimed accuracy of SuperCOSMOS (Hambly et al. 2001). While the mean difference in declination is negligible, the difference in right ascension marginally exceeds the $3\text{-}\sigma$ level.

A similar radio-optical comparison was carried out for seven of the eight probable BL Lac objects, excluding IVS B1923+210 which was too faint to be seen with SuperCOSMOS. The mean differences were not significant, with a $1\text{-}\sigma$ scatter of $0''.15$ in each coordinate. This result supports the identifications and hence their classification as BL Lac objects.

5. Summary and conclusion

We performed spectroscopic observations of the optical counterparts of 47 southern radio sources from the ICRF and measured 31 new redshifts, with two of them having $z \geq 3$. At least two emission lines were confidently identified for each target. Redshifts were

determined principally from isolated lines, with lines that were weak, blended or affected by strong absorption given lower (or zero) weight. Eight targets showed featureless spectra, and were considered as BL Lac objects.

There were eight ICRF2 defining radio sources in this run. Five of them — IVS B1659–621, B1758–651, B1815–553, B2236–572 and B2344–514— were confirmed as extragalactic sources. Source IVS B1631–810 was confirmed as a BL Lac object with a featureless spectrum, but two other sources, IVS B0107–610 and IVS B1443–162, were observed in poor weather conditions, and no emission lines could be confidently identified in their spectra.

This paper is based on observations collected at the European Organisation for Astronomical Research in the Southern Hemisphere, Chile, programme 058.A-0855(A). Two of us, Titov and Jauncey, were supported by a travel grant from the Australian Nuclear Science Technology Organisation (ANSTO) in their Access to Major Research Facilities Program (AMRFP) (reference number AMRFP 10/11-O-04) to travel to La Silla. The paper is published with the permission of the CEO, Geoscience Australia.

Facilities: NTT (GMOS)

REFERENCES

- Fey, A., Gordon, G., & Jacobs, C. (eds.), 2009, The Second realization of the International Celestial Reference Frame by Very Long Baseline Interferometry, IERS Technical Notes 35.
- Gearhart, M.R., Lund, J., Frantz, D., Kraus, J., 1972, *AJ*, 77, 557
- Halpern, J.P., Erakleous, M., & Matrox, J.R., 2003, *AJ*, 125, 573
- Hambly, N. C., Davenhall, A. C., Irwin, M. J. and MacGillivray, H. T., 2001, *MNRAS*, 326, 1315
- Jauncey, L.D., Batty, M.J., Gulkis, S. and Savage, A., 1982, *AJ*, 87, 763
- Jones, D. H., et al., 2009, *MNRAS*, 399, 683
- Ma, C., et al., 1998, *AJ*, 116, 516
- Maslennikov, K., Boldycheva, A., Malkin, Z., Titov, O., 2010, *Astrophysics*, 53, 147
- McCarthy, D. & Petit G. (eds.), 2004, IERS Conventions (2003), IERS Technical Notes 32, Verlag des Bundesamts für Kartographie und Geodäsie, Frankfurt am Main
- Ojha, R., et al., 2005, *AJ*, 130, 2529
- Preston, R.A., Morabito, D.D., Williams, J.G., Faulkner, J., Jauncey, D.L., Nicolson, G.D., 1985, *AJ*, 90, 1599
- Quiniento, Z. M. & Cersosimo, J. C. 1993, *A&AS*, 97, 435
- Reynolds, J.E., Jauncey, D.L., Russell, J.L., King, E.A., McCulloch, P.M., Fey, A.L, Johnston, K.J., 1994, *AJ*, 108, 725
- Schlüter, W. & Behrend D. 2007, *JG*, 81, 379

Titov, O., & Malkin, Z. 2009, *A&A*, 506, 1477

Wright, A.E., Wark, R.M., Troup, E., Otrupcek, R., Jennings, D., Hunt, A., Cooke, D.J.,
1991, *MNRAS*, 251, 330

Table 1. Outcomes of the spectroscopic observations

Source	RA (J2000) ^a	Dec (J2000) ^a	Redshift
IVS B0002–170	00 05 17.933	–16 48 04.678	0.7804 ± 0.0013
IVS B0008–300	00 10 45.177	–29 45 13.177	2.3439 ± 0.0052
IVS B0028–396	00 31 24.331	–39 22 49.391	1.2978 ± 0.0023
IVS B0034–220	00 37 14.825	–21 45 24.714	2.5133 ± 0.0021
IVS B0055–059	00 58 05.066	–05 39 52.277	1.2456 ± 0.0008
IVS B0107–610	01 09 15.475	–60 49 48.460	low S/N
IVS B0110–668	01 12 18.912	–66 34 45.187	1.1888 ± 0.0021
IVS B0122–260	01 25 18.837	–25 49 04.390	BL Lac
IVS B0221–171	02 23 43.763	–16 56 37.701	1.0152 ± 0.0017
IVS B1443–162	14 45 53.376	–16 29 01.619	BL Lac
IVS B1452–168	14 55 02.811	–17 00 13.953	low S/N
IVS B1505–304	15 08 52.993	–30 36 29.430	3.3684 ± 0.0023
IVS B1511–476	15 14 40.024	–47 48 29.858	1.5512 ± 0.0018
IVS B1533–316	15 36 54.498	–31 51 15.135	BL Lac
IVS B1633–810	16 42 57.346	–81 08 35.070	BL Lac
IVS B1635–141	16 38 45.284	–14 15 50.237	0.2575 ± 0.0004
IVS B1647–296	16 50 39.544	–29 43 46.955	low S/N
IVS B1659–621	17 03 36.541	–62 12 40.008	1.7547 ± 0.0012
IVS B1707–038	17 10 17.205	–03 55 50.128	1.9231 ± 0.0017
IVS B1726–038	17 28 50.235	–03 50 50.436	0.6617 ± 0.0003
IVS B1748–253	17 51 51.263	–25 24 00.064	star

Table 1—Continued

Source	RA (J2000) ^a	Dec (J2000) ^a	Redshift
IVS B1758–651	18 03 23.496	–65 07 36.761	1.1991 ± 0.0006
IVS B1815–553	18 19 45.399	–55 21 20.745	1.6292 ± 0.0013
IVS B1822–173	18 25 36.532	–17 18 49.848	star
IVS B1852–534	18 57 00.452	–53 25 00.356	0.7779 ± 0.0007
IVS B1923+210	19 25 59.605	+21 06 26.162	BL Lac
IVS B1928–698	19 33 31.159	–69 42 58.914	1.4807 ± 0.0020
IVS B1936–623	19 41 21.769	–62 11 21.056	low S/N
IVS B2012–017	20 15 15.158	–01 37 32.560	BL Lac
IVS B2053–323	20 56 25.070	–32 08 47.801	BL Lac
IVS B2059–786	21 05 44.961	–78 25 34.547	low S/N
IVS B2107–105	21 10 00.978	–10 20 57.319	2.5004 ± 0.0012
IVS B2117–614	21 21 04.074	–61 11 24.624	1.0168 ± 0.0011
IVS B2135–184	21 38 41.928	–18 10 44.371	0.1887 ± 0.0001
IVS B2158–167	22 00 54.878	–16 32 32.701	0.8355 ± 0.0024
IVS B2211–388	22 14 38.569	–38 35 45.008	0.3888 ± 0.0004
IVS B2220–163	22 23 41.172	–16 07 05.188	0.8811 ± 0.0002
IVS B2234–253	22 37 18.355	–25 06 32.519	1.2788 ± 0.0011
IVS B2236–572	22 39 12.075	–57 01 00.839	0.5686 ± 0.0023
IVS B2239–631	22 43 07.839	–62 50 57.322	0.3924 ± 0.0005
IVS B2254–204	22 56 41.208	–20 11 40.510	BL Lac
IVS B2300–307	23 03 05.821	–30 30 11.473	star

Table 1—Continued

Source	RA (J2000) ^a	Dec (J2000) ^a	Redshift
IVS B2318–087	23 21 18.250	–08 27 21.521	3.1639 ± 0.0033
IVS B2321–065	23 23 39.113	–06 17 59.238	2.1440 ± 0.0020
IVS B2327–459	23 30 37.680	–45 39 58.101	0.4471 ± 0.0004
IVS B2344–514	23 47 19.864	–51 10 36.065	1.7502 ± 0.0060
IVS B2354–251	23 57 23.850	–24 51 03.163	1.6137 ± 0.0014

^aICRF2 radio position

Table 2. Observed emission lines

Source	Line	λ_{rest} (Å)	λ_{obs} (Å) ^a	z	mean z
IVS B0002–170	[O II]	2470.2	4398.0	0.7804	0.7804 ± 0.0013
	Mg II	2797.9	4986.9	0.7824	
	[Ne V]	3425.5	6086.4	0.7768	
	H γ	4340.5	7715.7:	0.7776	
	[O III]	4363.2	7765.4:	0.7797	
	H β	4861.3	8673.7	0.7842	
	[O III]	4958.9	8840.4:	0.7827	
	[O III]	5006.8	8904.4	0.7784	
IVS B0008–300	Ly α	1215.7	4090.0:	2.3644	2.3439 ± 0.0052
	N V	1240.1	4176.4:	2.3677	
	Si IV	1396.8	4683.9	2.3534	
	C IV	1549.1	5167.0	2.3356	
	C III]	1908.7	6380.1	2.3426	
IVS B0028–396	C III]	1908.7	4381.4	1.2955	1.2978 ± 0.0023
	Mg II	2797.9	6435.4	1.3001	
IVS B0034–220	Ly α	1215.7	4276.2	2.5176	2.5133 ± 0.0021
	N V	1240.1	4355.3:	2.5120	
	Si IV	1396.8	4909.6	2.5150	
	C IV	1549.1	5441.7	2.5129	
	C III]	1908.7	6695.6	2.5079	
IVS B0055–059	C III]	1908.7	4287.5	1.2463	1.2456 ± 0.0008
	Mg II	2797.9	6284.2	1.2460	

Table 2—Continued

Source	Line	λ_{rest} (Å)	λ_{obs} (Å) ^a	z	mean z
IVS B0110–668	[O II]	3726.8	8364.9	1.2446	
	C III]	1908.7	4174.2	1.1869	1.1888 ± 0.0021
	Mg II	2797.9	6129.1	1.1906	
IVS B0221–171	C III]	1908.7	3840.8	1.0122	1.0152 ± 0.0017
	Mg II	2797.9	5639.3	1.0155	
	H γ	4340.5	8758.9	1.0180	
IVS B1505–304	Ly lim	911.5	4031.2:	3.4226	3.3684 ± 0.0023
	Ly β	1025.7	4524.4:	3.4110	
	Ly α	1215.7	5412.6:	3.4524	
	N V	1240.1	5466.2:	3.4077	
	Si IV	1396.8	6095.4	3.3639	
	C IV	1549.1	6770.2	3.3705	
	C III]	1908.7	8342.4	3.3707	
	C IV	1549.1	3957.3	1.5546	1.5512 ± 0.0018
IVS B1511–476	He II	1640.4	4185.6	1.5515	
	C III]	1908.7	4859.9	1.5461	
	Mg II	2797.9	7142.2	1.5527	
	[Ne V]	3345.4	4206.9	0.2575	0.2575 ± 0.0004
IVS B1635–141	[Ne V]	3425.5	4315.8	0.2599	
	[O II]	3726.0	4682.7	0.2568	
	[Ne III]	3869.1	4868.1	0.2582	
	[Ne III]	3967.8	4987.0	0.2569	

Table 2—Continued

Source	Line	λ_{rest} (Å)	λ_{obs} (Å) ^a	z	mean z
	H δ	4101.7	5155.7	0.2570	
	H γ	4340.5	5466.8	0.2595	
	H β	4861.3	6111.1	0.2571	
	[O III]	4958.9	6229.7	0.2563	
	[O III]	5006.8	6289.7	0.2562	
	H α	6562.8	8233.8:	0.2546	
	[N II]	6583.5	8267.3:	0.2558	
IVS B1659–621	Si IV	1396.8	3845.5	1.7532	1.7547 ± 0.0012
	C IV	1549.1	4269.0	1.7559	
	C III]	1908.7	5253.0	1.7521	
	Mg II	2797.9	7716.0	1.7578	
IVS B1707–038	C IV	1549.1	4523.0	1.9199	1.9231 ± 0.0017
	C III]	1908.7	5584.3	1.9256	
	Mg II	2797.9	8180.6	1.9238	
IVS B1726–038	Mg II	2797.9	4647.3	0.6610	0.6617 ± 0.0003
	[Ne V]	3345.4	5559.8	0.6619	
	[Ne V]	3425.5	5689.8	0.6610	
	[O II]	3726.8	6195.7	0.6625	
	[Ne III]	3869.1	6428.5	0.6615	
	[Ne III]	3967.8	6590.6	0.6610	
	H γ	4340.5	7212.0	0.6616	
	H β	4861.3	8077.8	0.6616	

Table 2—Continued

Source	Line	λ_{rest} (Å)	λ_{obs} (Å) ^a	z	mean z
IVS B1758–651	[O III]	4958.9	8246.2	0.6629	1.1991 ± 0.0006
	[O III]	5006.8	8321.9	0.6621	
	C III]	1908.7	4199.1	1.2000	
	C II]	2326.9	5117.0	1.1990	
	[Ne IV]	2423.8	5327.0	1.1977	
	Mg II	2797.9	6156.8	1.2005	
	[Ne V]	3345.4	7331.9:	1.1916	
	[Ne V]	3425.5	7527.8	1.1976	
IVS B1815–553	[O II]	3726.8	8197.9	1.1997	1.6292 ± 0.0013
	C IV	1549.1	4070.3	1.6276	
	C III]	1908.7	5016.8	1.6284	
	C II]	2326.9	6123.7	1.6317	
	Mg II	2797.9	7384.2:	1.6391	
IVS B1852–534	Mg II	2797.9	4973.4	0.7775	0.7779 ± 0.0007
	[O II]	3726.8	6628.4	0.7786	
	H δ	4101.7	7280.6	0.7750	
	H γ	4340.5	7715.9	0.7777	
	[O III]	4958.9	8830.3	0.7807	
	[O III]	5006.8	8900.6	0.7777	
	C IV	1549.1	3836.7	1.4768	
IVS B1928–698	C III]	1908.7	4730.3	1.4782	1.4807 ± 0.0020
	C II]	2326.9	5755.2:	1.4733	

Table 2—Continued

Source	Line	λ_{rest} (Å)	λ_{obs} (Å) ^a	z	mean z
IVS B2107–105	Mg II	2797.9	6952.9	1.4850	2.5004 ± 0.0012
	[Ne V]	3345.4	8306.2	1.4829	
	Ly α	1215.7	4258.3	2.5028	
	N V	1240.1	4347.6	2.5057	
	Si IV	1396.8	4889.9	2.5009	
	C IV	1549.1	5418.5	2.4979	
IVS B2117–614	C III]	1908.7	6680.4	2.4999	1.0168 ± 0.0011
	C III]	1908.7	3848.3	1.0161	
	C II]	2326.9	4685.5	1.0136	
	Mg II	2797.9	5651.2	1.0198	
	[O II]	3726.8	7514.2	1.0163	
	H γ	4340.5	8760.6	1.0184	
IVS B2135–184	[O II]	3727.7	4430.9	0.1887	0.1887 ± 0.0001
	[Ne III]	3869.1	4598.4	0.1885	
	Ca H	3934.8	4680.8	0.1896	
	Ca K	3969.6	4718.1	0.1886	
	H γ	4340.5	5158.2	0.1884	
	H β	4861.3	5778.3	0.1886	
	[O III]	4958.9	5889.4	0.1876	
	[O III]	5006.8	5949.7	0.1883	
	Na D	5892.9	7005.7	0.1888	
	H α	6562.8	7805.7	0.1894	

Table 2—Continued

Source	Line	λ_{rest} (Å)	λ_{obs} (Å) ^a	z	mean z
	[S II]	6716.4	7986.3	0.1891	
IVS B2158–167	Mg II	2797.9	5142.3	0.8379	0.8355 ± 0.0024
	[O III]	5006.8	9178.2	0.8331	
IVS B2211–388	[O II]	3727.7	5180.5	0.3897	0.3888 ± 0.0004
	H β	4861.3	6747.3:	0.3880	
	[O III]	4958.9	6886.8:	0.3888	
	[O III]	5006.8	6954.6	0.3890	
	H α	6562.8	9108.5	0.3879	
	[N II]	6583.5	9140.3	0.3884	
IVS B2220–163	C II]	2326.9	4385.4:	0.8846	0.8811 ± 0.0002
	Mg II	2797.9	5262.7	0.8809	
	[O II]	3726.8	7011.9	0.8815	
	[Ne III]	3869.1	7277.4	0.8809	
IVS B2234–253	C III]	1908.7	4347.3	1.2776	1.2788 ± 0.0011
	Mg II	2797.9	6379.3	1.2800	
IVS B2236–572	Mg II	2797.9	4381.2	0.5659	0.5686 ± 0.0023
	[Ne V]	3425.5	5388.8	0.5731	
	[O II]	3726.8	5838.7	0.5667	
IVS B2239–631	Mg II	2797.9	3901.5	0.3944	0.3924 ± 0.0005
	[Ne V]	3345.4	4649.6:	0.3898	
	[Ne V]	3425.5	4774.9	0.3939	
	[Ne III]	3869.1	5385.5	0.3919	

Table 2—Continued

Source	Line	λ_{rest} (Å)	λ_{obs} (Å) ^a	z	mean z
IVS B2318–087	H γ	4340.5	6056.1:	0.3953	3.1639 ± 0.0033
	H β	4861.3	6767.9	0.3922	
	[O III]	4958.9	6899.8	0.3914	
	[O III]	5006.8	6968.1	0.3917	
	H α	6562.8	9129.7	0.3911	
	Ly α	1215.7	5065.5	3.1668	
IVS B2321–065	C IV	1549.1	6445.6	3.1610	2.1440 ± 0.0020
	C III]	1908.7	7976.2:	3.1788	
	Ly α	1215.7	3820.9	2.1430	
	N V	1240.1	3901.7:	2.1462	
	Si IV	1396.8	4414.6:	2.1606	
	C IV	1549.1	4865.6	2.1410	
IVS B2327–459	C III]	1908.7	5970.9:	2.1282	0.4471 ± 0.0004
	Mg II	2797.9	8807.9	2.1480	
	Mg II	2797.9	4051.8	0.4482	
	[O II]	3726.8	5392.7	0.4470	
	H β	4861.3	7033.7	0.4469	
	[O III]	4958.9	7169.0:	0.4457	
IVS B2344–514	[O III]	5006.8	7242.4	0.4465	1.7502 ± 0.0060
	Si IV	1396.8	3873.2:	1.7730	
	C IV	1549.1	4250.8	1.7441	
	C III]	1908.7	5261.0	1.7563	

Table 2—Continued

Source	Line	λ_{rest} (Å)	λ_{obs} (Å) ^a	z	mean z
IVS B2354–251	Mg II	2797.9	7700.3:	1.7521	1.6137 ± 0.0014
	C IV	1549.1	4045.2	1.6114	
	C III]	1908.7	4992.4	1.6156	
	Mg II	2797.9	7314.0	1.6141	

^aA colon after the observed wavelength indicates that the line position was uncertain, because of blending, proximity to a noise spike, or associated absorption, and hence was not used to determine the redshift

Table 3: Comparison between radio and optical positions for the stellar misidentifications

Source	ICRF2 position			Optical position		$\Delta\alpha$	$\Delta\delta$	σ_{opt}			
	J2000			J2000		ICRF2–optical					
	h	m	s	°	'	″	s	″	″		
IVS B1748–253	17	51	51.263	–25	24	00.06	51.104	01.44	2.15	1.38	0.29
IVS B1822–173	18	25	36.532	–17	18	49.85	36.566	50.57	–0.49	0.72	0.21
IVS B1923+210	19	25	59.605	+21	06	26.16	59.662	24.37	–0.80	–1.79	0.22
IVS B2300–307	23	03	05.821	–30	30	11.47	05.897	15.06	–0.98	3.59	0.15

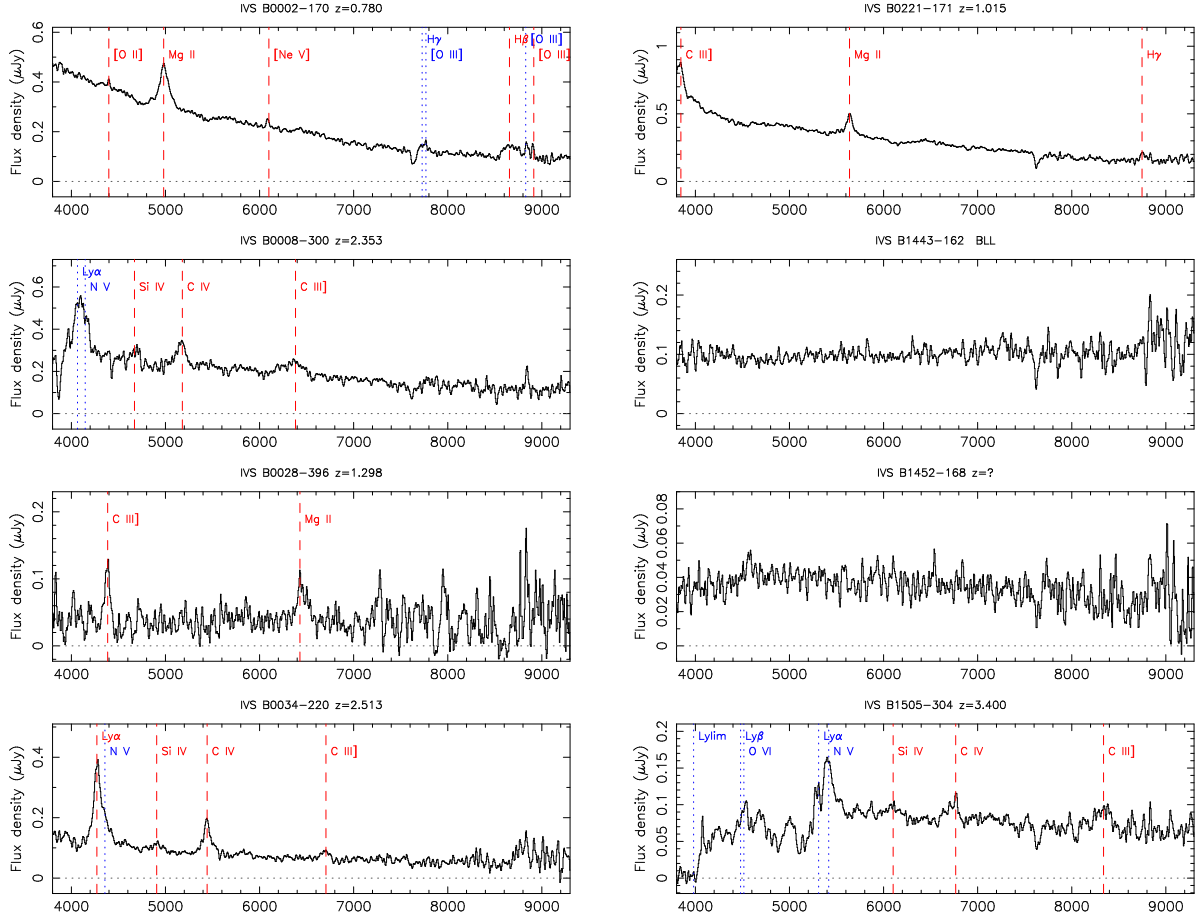


Fig. 1.— Optical spectra for 44 IVS targets, including 31 emission-line objects listed in Table 2, eight possible BL Lac objects, and five low signal-to-noise spectra that could not be classified. Dashed lines indicate emission lines used for redshift determination; dotted lines indicate features that were not used.

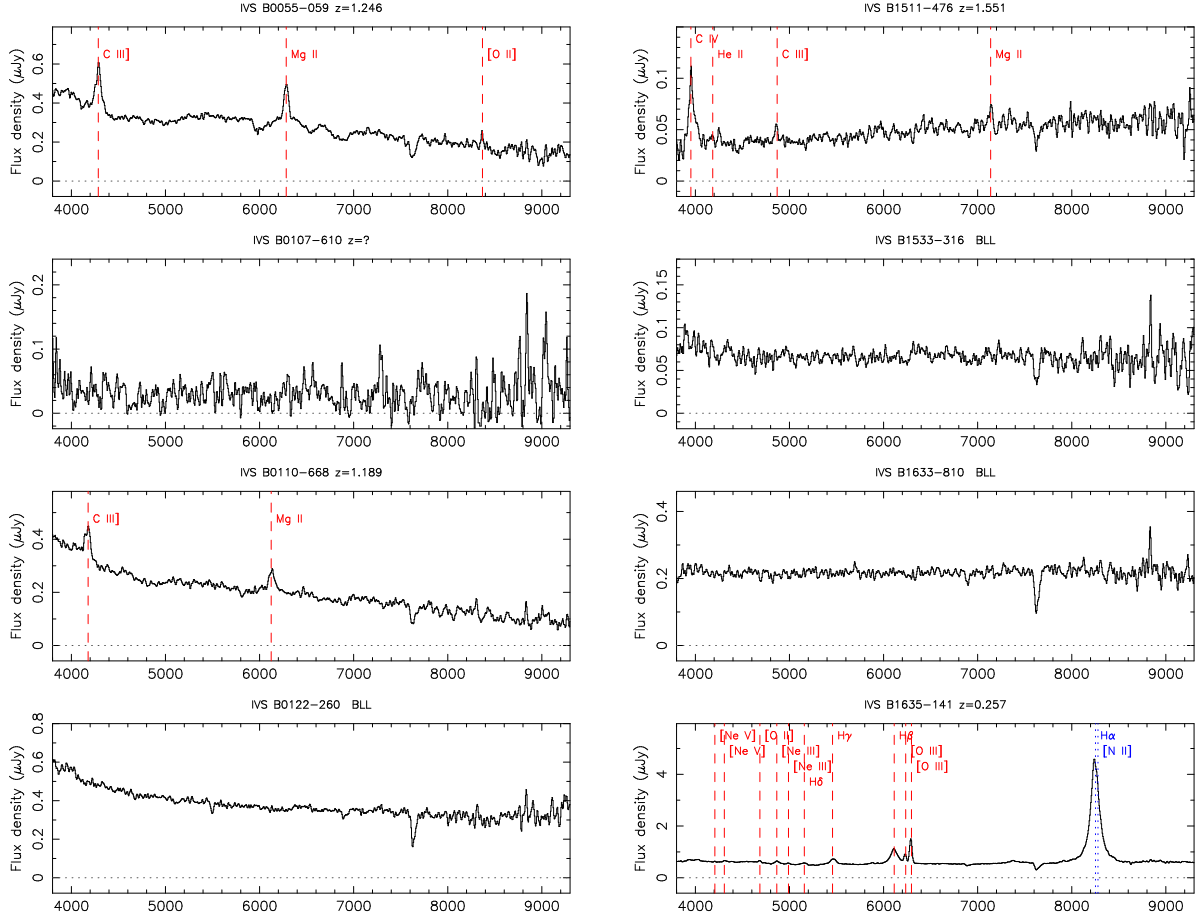


Fig. 1 (continued).—

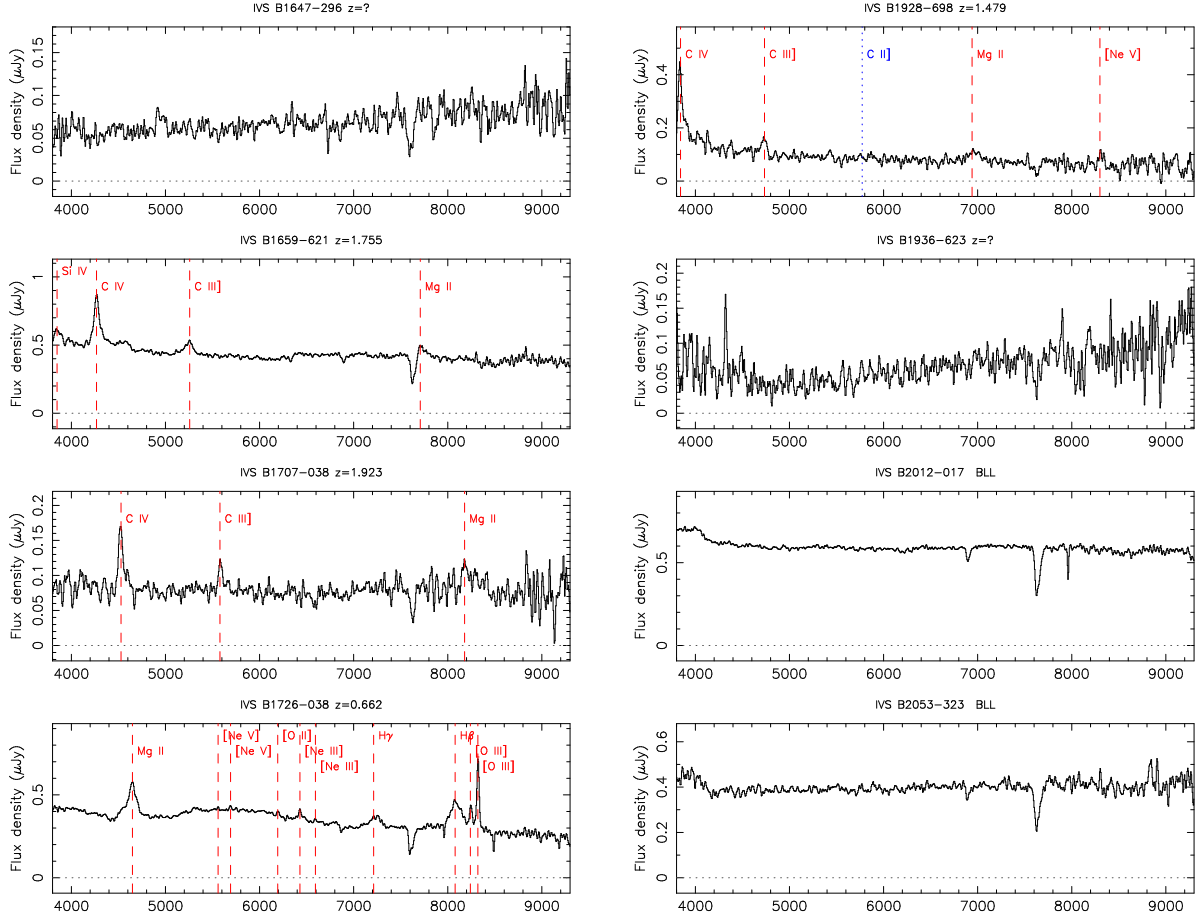


Fig. 1 (continued).—

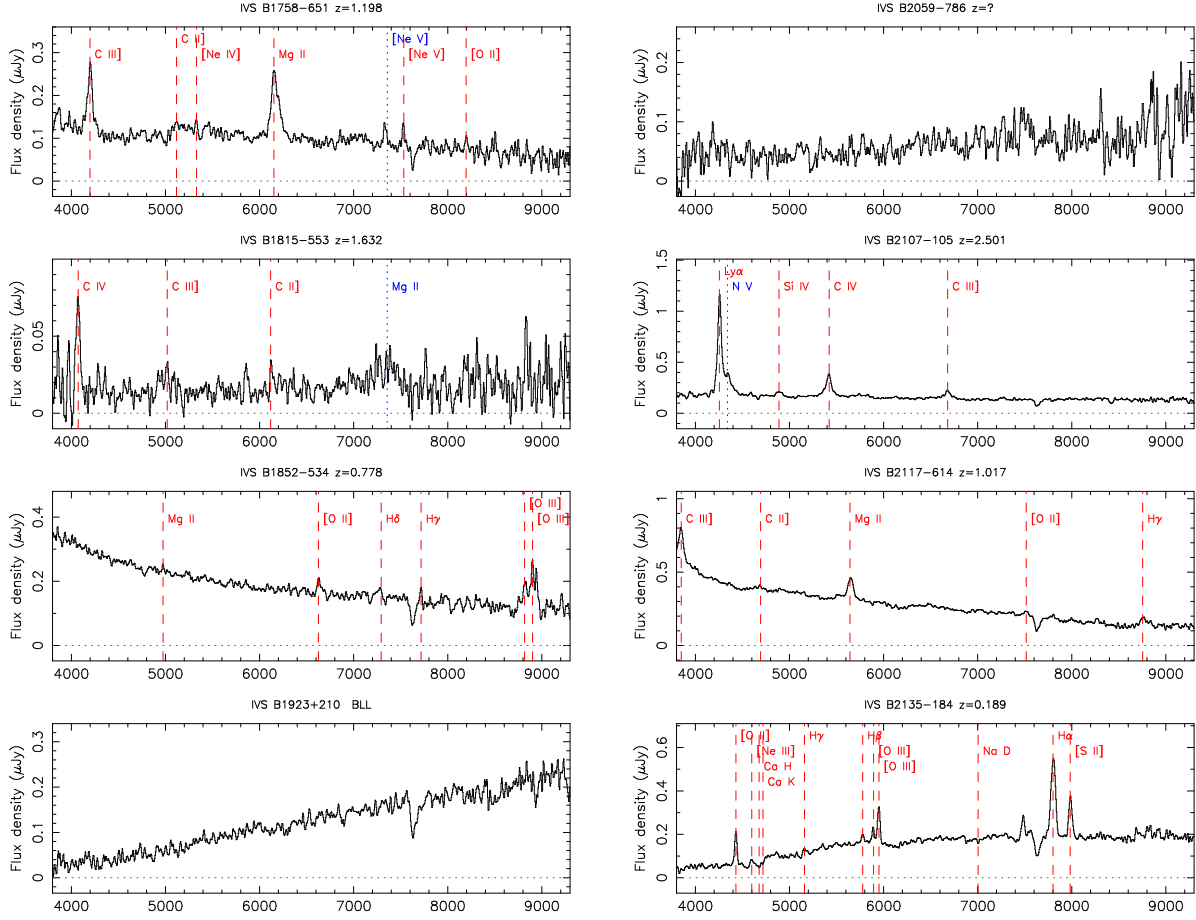


Fig. 1 (continued).—

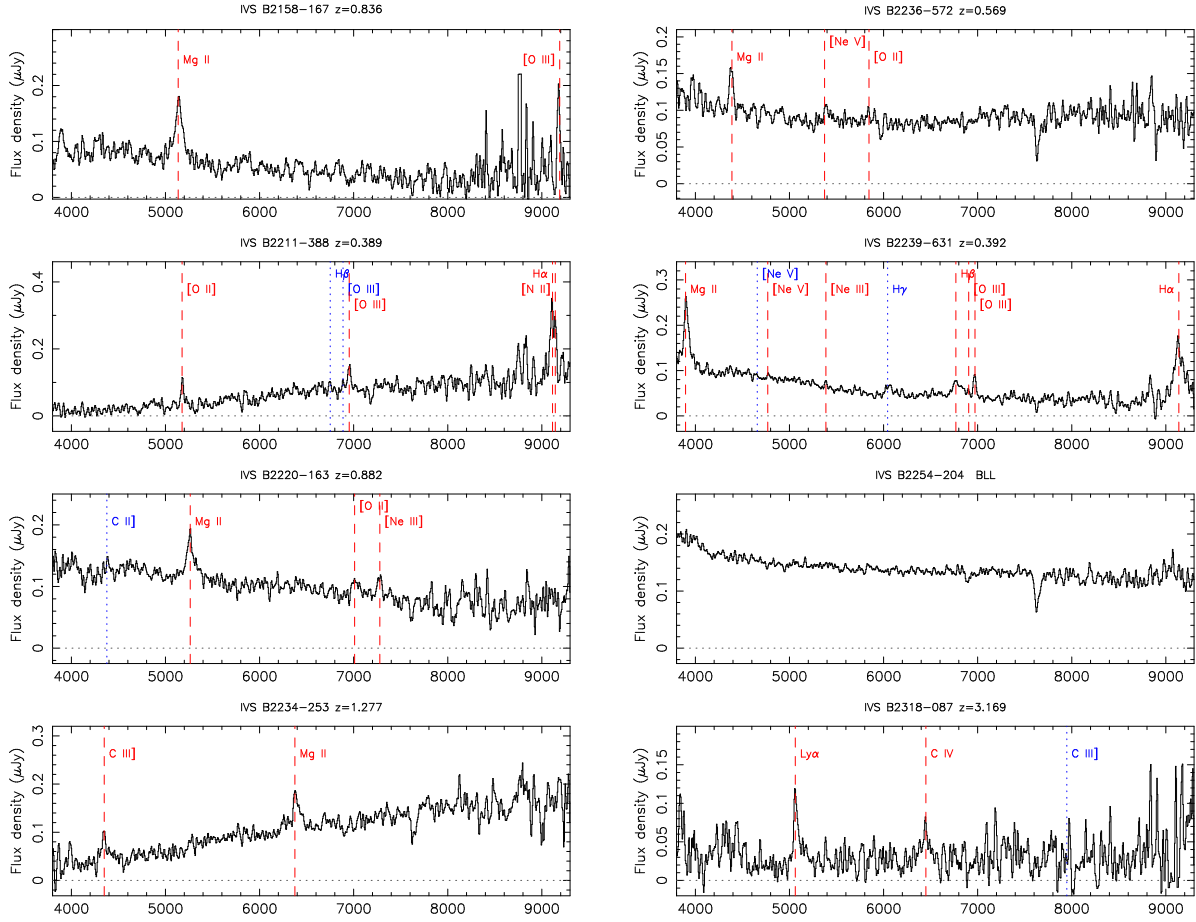


Fig. 1 (continued).—

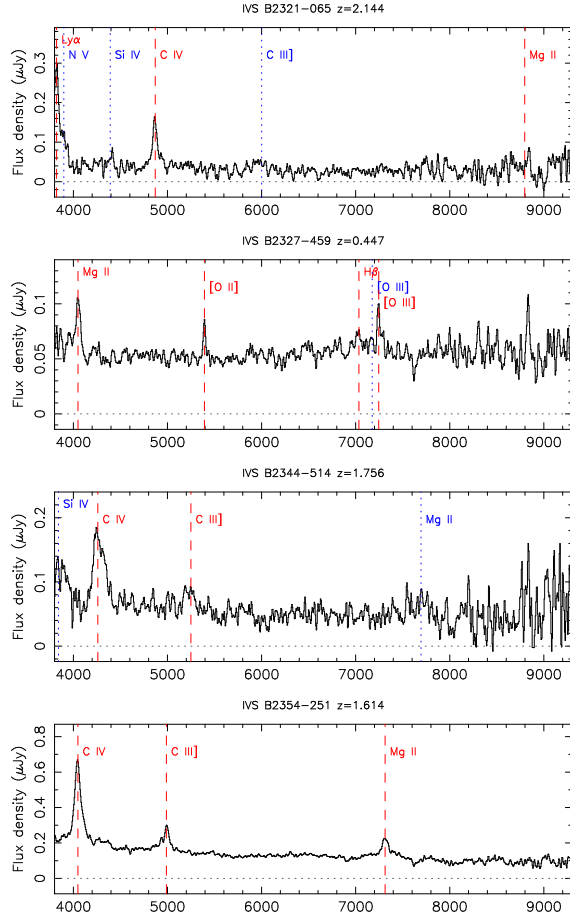


Fig. 1 (continued).—

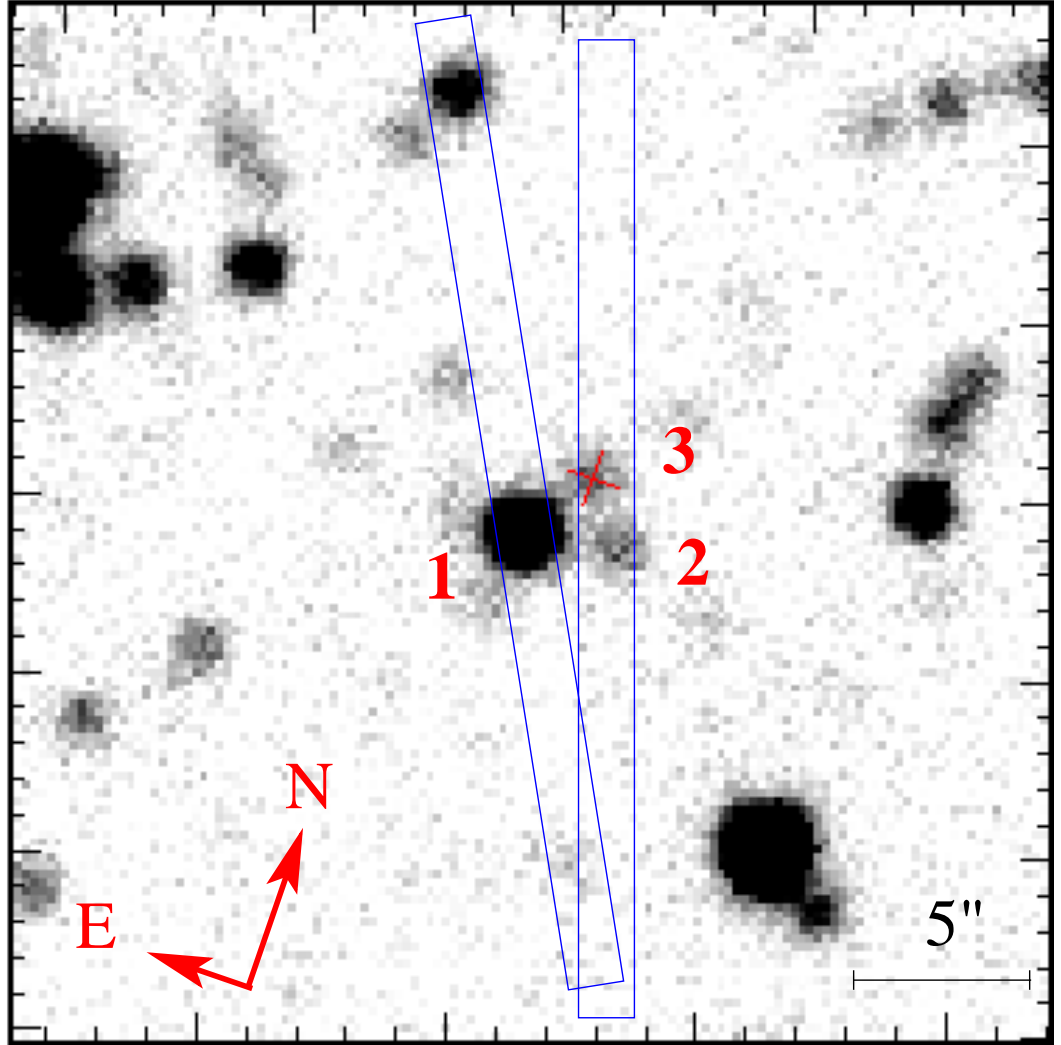


Fig. 2.— NTT acquisition image of the area near the radio position of the source IVS B1923+210. The optical identification is object 3, marked with a red cross; objects 1 and 2 showed stellar spectra. The two slit positions used are marked by blue boxes.

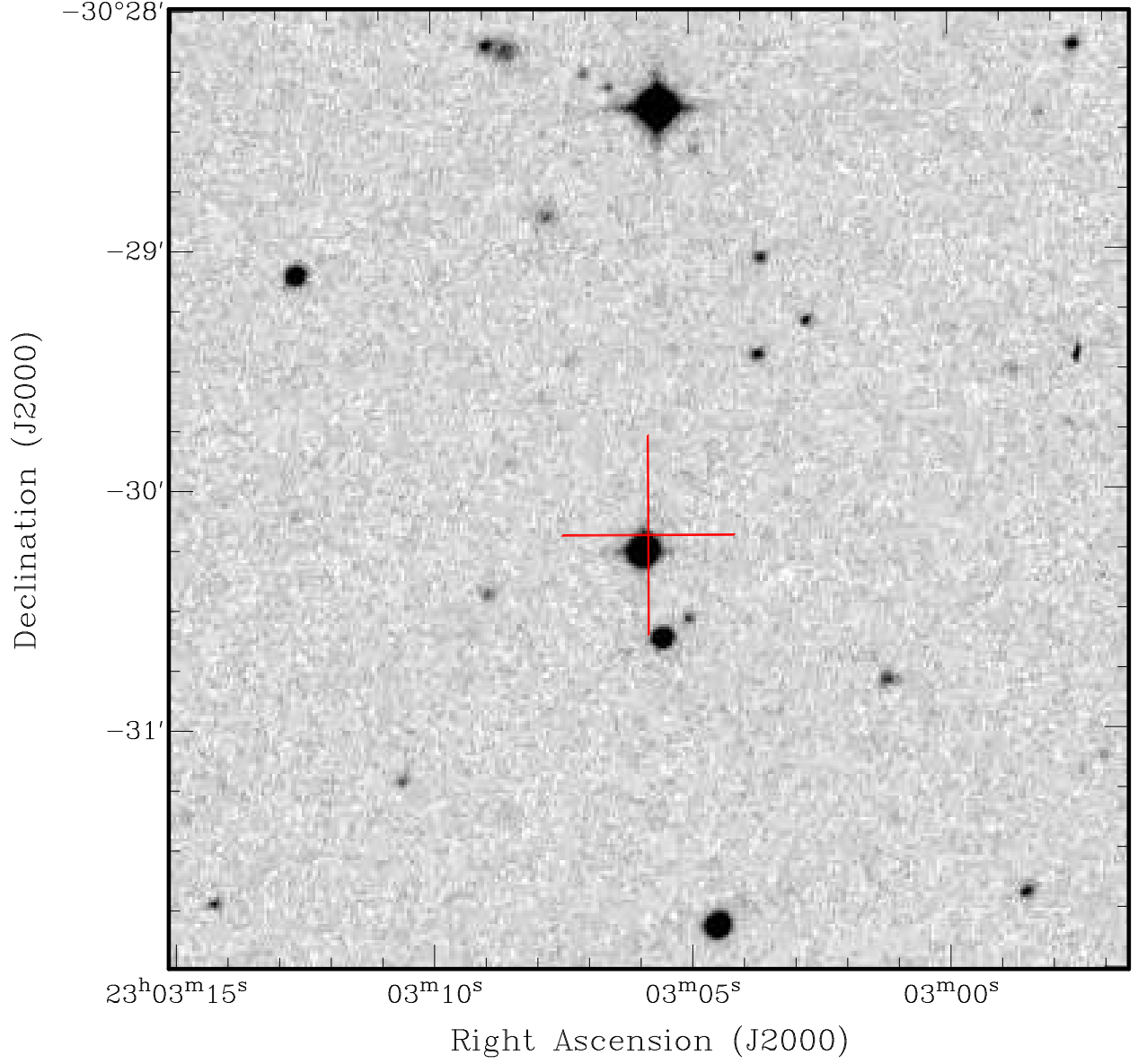


Fig. 3.— Finding chart for the source IVS B2300–307 from the UK Schmidt B image. The IVS position is marked with a cross, showing how the optical field of the radio source is obscured by the foreground star.